A Programmable Nonlinear Acoustic Metamaterial

Tianzhi Yang[1,2,3], Zhi-Guang Song[2], Eoin Clerkin[2], Ye-Wei Zhang[3], Jia-He Sun[3], Yi-Shu Su[3], Li-Qun Chen[1]*, and Peter Hagedorn[2]

1. Shanghai Institute of Applied Mathematics and Mechanics, Shanghai University, Shanghai, 200072, China

2. Dynamics and Vibrations Group, Numerical Methods in Mechanical Engineering, Technische Universite at Darmstadt, Dolivostr. 15, Darmstadt 64293, Germany.

3. Department of Astronautics, Shenyang Aerospace University, Shenyang 110136, China

Abstract:

Acoustic metamaterials with specifically designed lattices can manipulate acoustic/elastic waves in unprecedented ways. Whereas there are many studies that focus on passive linear lattice, with non-reconfigurable structures. In this letter, we present the design, theory and experimental demonstration of an **active nonlinear** acoustic metamaterial, the dynamic properties of which can be modified instantaneously with reversibility. By incorporating active and nonlinear elements in a single unit cell, a real-time tunability and switchability of the band gap is achieved. In addition, we demonstrate a dynamic "editing" capability for shaping transmission spectra, which can be used to create the desired band gap and resonance. This feature is impossible to achieve in passive metamaterials. These advantages demonstrate the versatility of the proposed device, paving the way toward smart acoustic devices, such as logic elements, diode and transistor.

INTRODUCTION

Metamaterials are man-made composites that control waves in ways that result in exotic behavior that are not available in natural materials, resulting in exotic behavior[1-2]. The acoustic metamaterials can manipulate waves with wavelengths much larger than the structural features of the system and have been successfully

applied in acoustic wave cloaking[3-5], imaging[6], wavefront modulation[7,8] and vibration control[9-14]. The extraordinary capability of acoustic metamaterials is bestowed by band gaps, within which elastic/acoustic waves experience strong attenuation. Band gaps are typically generated from two main mechanisms, namely Bragg scattering[15] and local resonance[16]. In most acoustic metamaterials, local resonance is the main mechanism. However, most acoustic metamaterials are comprised of passive building blocks, such as internal resonators, which restricts the tunability during operation. Therefore, once fabricated, structural modification is difficult and the devices are severely limited by their original design.

Soft metamaterials are very promising for overcoming this difficulty, and they have recently received increased attention for their unusual properties[17-19]. When these structures are subjected to an external load, significant phase transitions can be switched in a sudden but controlled manner. Such media are expected to offer new opportunities to manipulate elastic waves and sound. Nevertheless, as local instability (buckling) is required in this strategy, large plastic deformations may occur, leading to an irreversible, relatively slow tunability. Moreover, this strategy often requires additional facilities to apply continuous external pressure during operation, inherently limiting their practical application. In this letter, we present an acoustic metamaterial that has a real-time reconfiguration capability to overcome these limitations.

In the literature, a number of active acoustic metamaterials have been proposed that may circumvent these limitations[20-28]. However, most of the active acoustic metamaterials are based on linear internal resonators[21-28] that operate in a narrow operation frequency range. Although a **nonlinear** acoustic metamaterial device has been theoretically proposed in Reference 29, there is no experimental demonstration in the literature known to the authors. In this letter, we describe a hybrid of active and nonlinear elements in a single metamaterial device. Specifically, some unexplored phenomena including real-time, programmable, reconfigurable band gaps and transition dynamics are unveiled.

Figure 1(a) shows a 1D acoustic metamaterial with ten periodic unit cells

fabricated out of polylactic acid (PLA, with Young's modulus is Es=3.5 GPa, Poisson's ratio μ_s=0.36, mass density ρ_s=1250 kg/m^3) using a 3D-printer (Replicator 2X, MakerBot). Figure 1(b) shows a typical implementation of a unit cell comprising two nonlinear independent internal resonators fixed in a 3D-printed square frame with a lattice constant a=65.1 mm, wall thickness t_s=2.2 mm and height h=20 mm. A pair of cylindrical electromagnets (radius R=10 mm, height h_c=15mm and mass m =20 g) are arranged 1.1 mm apart and mounted on the two curved beams, acting as controllable internal resonators. A DC current supply powers the unit cells, each of which is connected to a switch. Therefore, each internal resonator can be controlled individually and continuously as desired.

DESIGN OF A NONLINEAR ACOUSTIC METAMATERIAL

The key element providing the nonlinear stiffness is the curved beam. The curved beam is the key element to support nonlinear stiffness. In the undeformed configuration, it has width $w_b = 20$mm, thickness $t_b = 1$ mm and height $h_b =$ 16mm. Experimental measurements of its deformation-displacement response [Figure 2(a)] establishes the stiffness characteristic, calculated from the slope of the curve, i.e. $k = \mathrm{dF/dx}$. The stiffness values were estimated in the range of 0 mm~0.6 mm, within which the constant k was calculated. Clearly, the stiffness of the beam increases monotonically with applied force and exhibits strong nonlinear hardening. Moreover, we found that the measured stiffness has a critical point at 0.32 *mm*, at which the stiffness value significantly alters around this value, forming a threshold between low and high stiffness. To rapidly switch between high and low stiffness, electrically switched electromagnets are adopted to generate the required deformation instantaneously. If the circuit is open, the two electromagnets are separated; the undeformed stiffness is measured to be k_{un}=~7900 N/m. In contrast, if the circuit is closed, the two electromagnets are rapidly join (~1s) and each nonlinear curved beam is displaced 0.55 mm, yielding a significantly large stiffness value: $k_{de} = \sim 59000$

N/m. Here we use "ON" and "OFF" to denote the deformed and undeformed configurations, behaving as coding elements of "1" and "0" [Figure 2(b)]. For coding the elements as 0000…., 1100, and 1111…., some interesting dynamical behavior develop.

Next, we analyzed numerically the propagation of an acoustic wave through the acoustic metamaterial. Assuming long wavelengths, the proposed 1D acoustic metamaterial was modeled as a sandwich beam with internal resonators. Therefore, the Timoshenko beam theory with internal resonators is used to analyze wave propagation. The equation of motion for transverse vibration for the "OFF" state can be expressed as[30-32]

$$GA(\frac{\partial^2 w}{\partial x^2}+\frac{\partial \varphi}{\partial x})-\rho A\frac{\partial^2 w}{\partial t^2}+\frac{k_{un}}{a}(v_1-2w-v_2)=0, \tag{1a}$$

$$EI\frac{\partial^2 \varphi}{\partial x^2}-GA(\frac{\partial w}{\partial x}+\varphi)-\rho I\frac{\partial^2 \varphi}{\partial t^2}=0, \tag{1b}$$

$$-\frac{m_1}{a}\frac{\partial^2 v_1}{\partial t^2}-\frac{k_{un}}{a}(v_1-w)=0, \tag{1c}$$

$$-\frac{m_2}{a}\frac{\partial^2 v_2}{\partial t^2}+\frac{k_{un}}{a}(w-v_2)=0, \tag{1d}$$

where *EI, GA, ρI,* and *ρA* are the bending rigidity, transverse shear rigidity, rotary inertia, and mass of the beam per unit length, respectively; *w* denotes the transverse displacement of the beam and φ denotes the rotation of the cross section, v_1 and v_2 are the oscillating displacements of the masses m_1 and m_2, respectively. For the experiment setup presented here, m_1=m_2=20 g. The effective material parameters of the acoustic metamaterial can be analyzed based on cellular solids theory[33,34], specifically, $E = E_s t_s/a$, $\rho = 2\rho_s t_s/a$, $\mu = \mu_s t_s/a$ and $\mathrm{G} = \mathrm{E}/2(1+\mu)$ with μ the effective Poisson's ratio.

For the "ON" state, the equation of motion for the deformed internal resonator becomes

$$GA(\frac{\partial^2 w}{\partial x^2}+\frac{\partial \varphi}{\partial x})-\rho A\frac{\partial^2 w}{\partial t^2}+\frac{2k_{de}}{a}(v_3-w)=0\,, \tag{2a}$$

$$EI\frac{\partial^2 \varphi}{\partial x^2}-GA(\frac{\partial w}{\partial x}+\varphi)-\rho I\frac{\partial^2 \varphi}{\partial t^2}=0\,, \tag{2b}$$

$$\frac{m_1+m_2}{a}\frac{\partial^2 v_3}{\partial t^2}+\frac{2k_{de}}{a}(v_3-w)=0\,, \tag{2c}$$

where v_3 is the displacement of the two attached electromagnets, which behaves as a new single resonator.

The displacement function in Eqs. (1) and (2) can be assumed to have the form

$$\begin{aligned} w(x,t) &= \hat{w}e^{i(qx-\omega t)},\\ \varphi(x,t) &= \hat{\varphi}e^{i(qx-\omega t)},\\ v_n(x,t) &= \hat{v}_n e^{i(qx-\omega t)}, \end{aligned} \tag{3}$$

in which $\hat{w}$, $\hat{\varphi}$, and $\hat{v}_n$ are the coefficients of displacement amplitude. The dispersion relation relating frequency ω to wave number q can be obtained by substituting Eq. (3) into Eqs. (1) and (2), respectively. Figure 3(a) shows the simulated dispersion relation between the first-three frequency branches. The dimensionless wave number is defined as $\bar{q}=aq$. A band gap has appeared between f=67-250 Hz in the "OFF" state, within which strong elastic wave attenuation takes place. In contrast, for the "ON" state, the acoustic wave in this range are allowed to propagate through the metamaterial [Figure 3(c)], indicating that the proposed device operates as an acoustic switch with a rapidly controllable response.

EXPERIMENTS

To validate the numerical simulation, we experimentally tested the dynamic response of the fabricated sample. To measure the transmission response, an elastic wave is harmonically excited through the metamaterial using an electrodynamic shaker (ETS type MPA409). Two tri-axial accelerometers (Brüel & Kjær type 4528-B) are adhesive-bonded to the top and bottom surfaces of the metamaterial. Both the input and output signal are recorded by a dynamic signal analyzer (LMS SCADAS),

which also provides the input signal to the shaker. Note that the normalized transmission spectrum $20\log_{10}\|A_{out}/A_{in}\|$ is calculated with A_{in} and A_{out} are the input and output amplitudes, respectively. Figure 3(b) and (d) shows the experimentally **measured** normalized transmission spectra for the OFF and ON state. These spectral data are in close agreements with the simulated data. The transmission is characterized by a drop of ~25 dB for *f*=75-80 Hz. In contrast, the measured results [Figure 3(d)] show the band gap from 75 to 80 Hz disappears as the Timoshenko beam theory predicts. Moreover, a new band gap from 262 to 300 Hz appears that is induced by the switching induced structural transformation of the internal resonator. Hence, the elastic wave propagates through the beam during OFF states and blocked during ON states.

We next demonstrate the real-time programmable response of the acoustic metamaterial device. We note that a programmable, **static** mechanical metamaterial was presented in Reference 35, our purpose is to force the metamaterial to generate a dynamic programmable response during operation. As indicated in Figure 4(a), we first switch on all the ten unit cells and then begin shaking the metamaterial, sweeping from 5 Hz to 350 Hz. We then gradually switch off the ten units during the sweeping process (within frequency *f*=5-100 Hz). The corresponding programmable transmission spectra [Fig. 4(a), orange line] shows a sequence of impulses, induced when the electromagnets detach suddenly. The continuous switching shapes the metamaterial to generate distinctly different transmission spectrum, as shown in blue line. Eventually, a new band gap appears between *f*=105-260 Hz, suggesting that switching between states is possible during operation.

In addition to band gap switching, we next demonstrate the dynamic "editing" capability of the resonance behavior. For reference, we measure the transmission spectrum between 5-20Hz, within which the first resonance occurs [Fig. 4(b)]. The blue and red lines denote the "ON" and "OFF" resonance, respectively. Starting from the "ON" state for all ten unit cells, we shake the metamaterial and sweep the frequency from 5 Hz. At 8.3 Hz, the spectra reach a peak value (the first natural

frequency). At this instance, we begin turning off all the unit cells sequentially. This results in a virtual resonance (yellow line) being created that is different from either the "ON" and "OFF" states. Furthermore, this new resonance curve has a wider frequency range and bridges the two states. This virtual resonance curve is not smooth, as it is induced by multiple impulses from sudden switching. This feature is impossible to achieve in passive metamaterial devices, providing an interesting unreported feature of our metamaterial, i.e., the capability to "edit" transmission spectra as desired. In contrast, conventional acoustic metamaterials such as cloaking devices, metasurfaces, and phononic crystals cannot be reconfigured after fabrication. Our device is very promising for overcoming this difficulty, we show that the structural transformation can be switched in a sudden but controlled manner. By designing and controlling more complex logic operations, more interesting functionalities are achievable. Such media are expected to offer new opportunities for smart filtering, trapping, guiding and manipulating of elastic waves[35-36] and sound[37].

CONCLUSIONS

We reported on the design, fabrication and experimental demonstration of the first nonlinear acoustic metamaterial, which has the capability to reversibly, and rapidly manipulate acoustic waves. Our results show that the electrically triggered deformations can control the nonlinear stiffness of internal resonators in an easier way, offering an alternative implementation of a nonlinear acoustic metamaterial. Moreover, it is capable of smart editing of transmission spectra. We expect applications to include low-frequency vibration isolation, sound filtering, and digital programmable materials.

Reference

[1]J. B. Pendry, D. Schurig, and D. R. Smith, Science, **312**, 1780 (2006).

[2]U. Leonhardt, Science, **312**, 1777 (2006).

[3]M. Brun, S. Guenneau, and A. B. Movchan, Appl. Phys. Lett. **94**, 061903 (2009).

[4]B. Popa, L. Zigoneanul, and S. A. Cummer, Phys. Rev. Lett. **106**, 253901 (2011).

[5]L. Zigoneanul, B. Popa, and S. A. Cummer, Nat. Mater. **13**, 352 (2014).

[6]B. Xie, Tang, H. Cheng, Z. Liu, S. Chen, and J. Tian, Adv. Mater. **29**, 1 (2017).

[7]Y. Xie, W. Wang, H. Chen, A. Konneker, B. I. Popa, and S. A. Cummer, Nat. Commun. **5,** 5553 (2014).

[8]J. Zhao, B. Li, Z. Chen, and C.W. Qiu, Appl. Phys. Lett. **103**, 151604 (2013).

[9]K. H. Matlack, A. Bauhofer, S. Krödel, A. Palermo, and C. Daraio, Proc Nat Acad Sci U S A, **113**, 8386. (2016).

[10]G. Ma, M. Yang, S. Xiao, Z. Yang, P. Sheng, Nat. mater. **13**, 873 (2014).

[11]G. L. Huang, and C. T. Sun, J. Vib. Acoust. **132**, 031003 (2010).

[12]R. Zhu, X. N. Liu, G. K. Hu, C. T. Sun, and G. L. Huang, J. Sound Vib. **333**, 2759 (2014).

[13]Y. F. Wang, Y. S. Wang, and X. X. Su, J. Appl. Phys. **110**, 113520 (2011).

[14]H. H. Huang, C. T. Sun, and G. L. Huang, Int. J. Eng. Sci. **47**, 610 (2009).

[15]J. Sánchez-Dehesa, V. Garcia-Chocano, D. Torrent, F. Cervera, S. Cabrera and S. Simon, J. Acoust. Soc. Am. **129**, 1173 (2011).

[16]Z Liu, X Zhang, Y Mao, YY Zhu, Z Yang, CT Chan, and P Sheng, science, **289**,1734 (2000).

[17]P. Wang, F. Casadei, S. Shan, J. C. Weaver, and K. Bertoldi, Phys. Rev. let. **113**, 014301 (2014).

[18] K. Bertoldi, and M. C. Boyce. Phys. Rev. B **77,** 052105 (2008)

[19]P. Wang, Y. Zheng, M. C. Fernandes, Y. Sun, K. Xu, S. Sun, and S. H. Kang, Phys. Rev. let. **118**, 084302 (2017)

[20]A. Bergamini, T. Delpero, L. D. Simoni, L. D. Lillo, M. Ruzzene, and P. Ermanni, Adv. Mater. **26**, 1343 (2014).

[21]R. Fleury, D. L. Sounas, C. F. Sieck, M. R. Haberman, and A. Alù, Science **343**, 516 (2014).

[22]W. Zhou, W. You, and L. Zuo, Smart Mater. Struct. **24**, 065021 (2015).

[23]S. Degraeve, C. Granger, B. Dubus, J. O. Vasseur, M. P. Thi, and A. C. Hladky, Smart Mater. Struct. **24**, 085013 (2015).

[24]Z. Wang, Q. Zhang, K Zhang, and G. K.Hu, Adv. Mater. **28**,9857 (2016).

[25]C. Sugino, S. Leadenham, M .Ruzzene, and A. Erturk, Smart Mater. Struct. **26**, 055029 (2017).

[26]A. Baz, New J. Phys. **11**, 123010 (2009).

[27]W. Akl, , and A. Baz, J. intelligent mater. systems struct. **21**, 541 (2010).

[28]Y. Y. Chen, G. L. Huang, and C. T. Sun, J. Vib. Acoust. **136**, 061008 (2014).

[29]J. M. Manimala, C. T. Sun, Acoust. Soc. Am. **139**, 3365 (2016).

[30]J. S. Chen, and Y. J. Huang, J. Vib. Acoust. **138**, 041009 (2016).

[31]J. S. Chen, B. Sharma, and C. T. Sun, Comp. Struct. **93**, 2120 (2011).

[32]J. S. Chen, and C. T. Sun. J. Sandwich Struct. Mater, **13**, 391 (2011).

[33]A. J. Wang, and D. L. McDowell, J. Eng. Mater. Tech. **126**, 2137 (2004).

[34]L. J. Gibson, M. F. Ashby, *Cellular solids*: structure and properties (Cambridge university press, 1997).

[35]B. Haghpanah, H. Ebrahimi, D. Mousanezhad, J. Hopkins, and A. Vaziri, Adv. Eng Mater. **18**, 643 (2015).

[35]R. Zhu, X. N. Liu, G. K. Hu, C. T. Sun and G. L. Huang, Nat. Comm. **5**, 5510 (2014).

[36]Y. Chen, M. Zheng, X. Liu, Y. Bi, Z. Sun, P. Xiang, J. Yang and G. Hu, Phys. Rev. B. **95**, 180104 (2017).

[37]J. Li, X. Zhou, G. Huang, G. Hu, Smart Mater. Struct. **25**, 045013 (2016).

Acknowledgement

The authors are grateful to the Alexander von Humboldt Foundation for offering fellowships to Dr. T-Z. Yang and Dr. Z.G. Song to carry out their research at Darmstadt University of Technology, Germany. T-Z. Yang, Y. W. Zhang and L.Q. Chen, acknowledge the support of National Science Foundation of China (Nos. 11672187 and 11572182) and Natural Science Foundation of Liaoning Province (201602573).

Figures

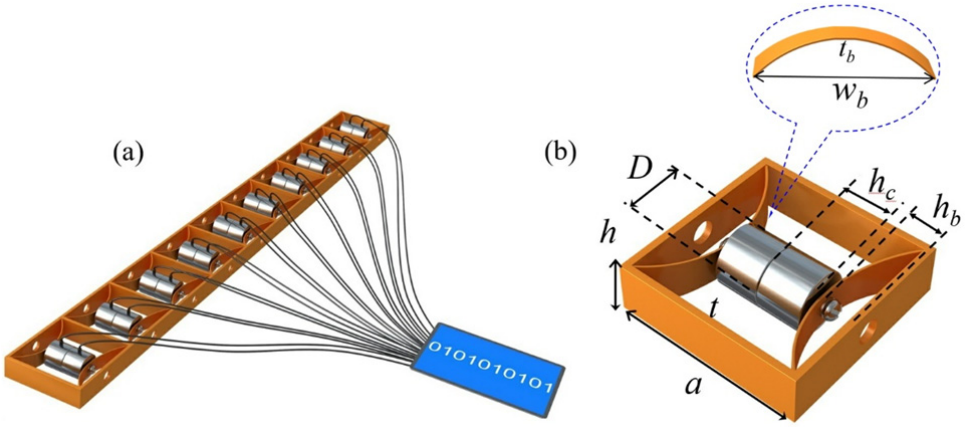

Figure 1. An electric-controlled programmable acoustic metamaterial. (a) The device comprises 10 unit cells and fabricated using 3D-printer and. Each cell is connected by an independent switch and the whole acoustic materials is controlled by a digital controller. (b) Close-up of a single unit cell comprising a square frame, two curved beam and a pair of electromagnets.

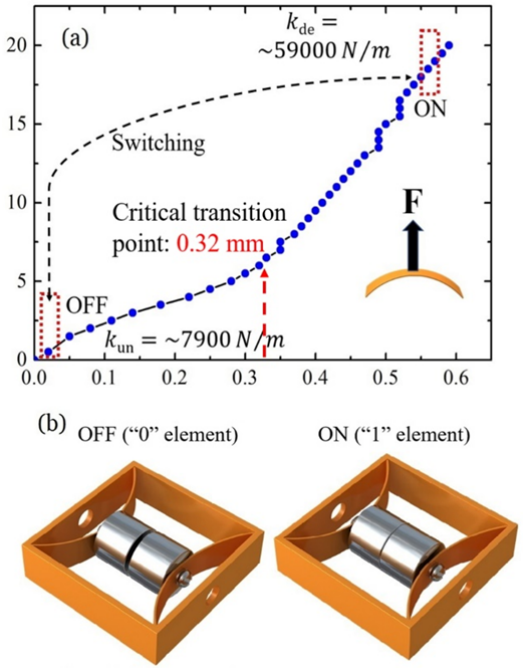

Figure 2. A 3D-printed unit cell. (a) Measured force-displacement relation of a curved beam. The effective stiffness is calculated from the slope of the curve. Inset shows the curved beam is subjected to an applied force F. (b) Attached and detached configuration of a single unit cell that as the '0' and '1' elements by switching "OFF" and "ON", respectively.

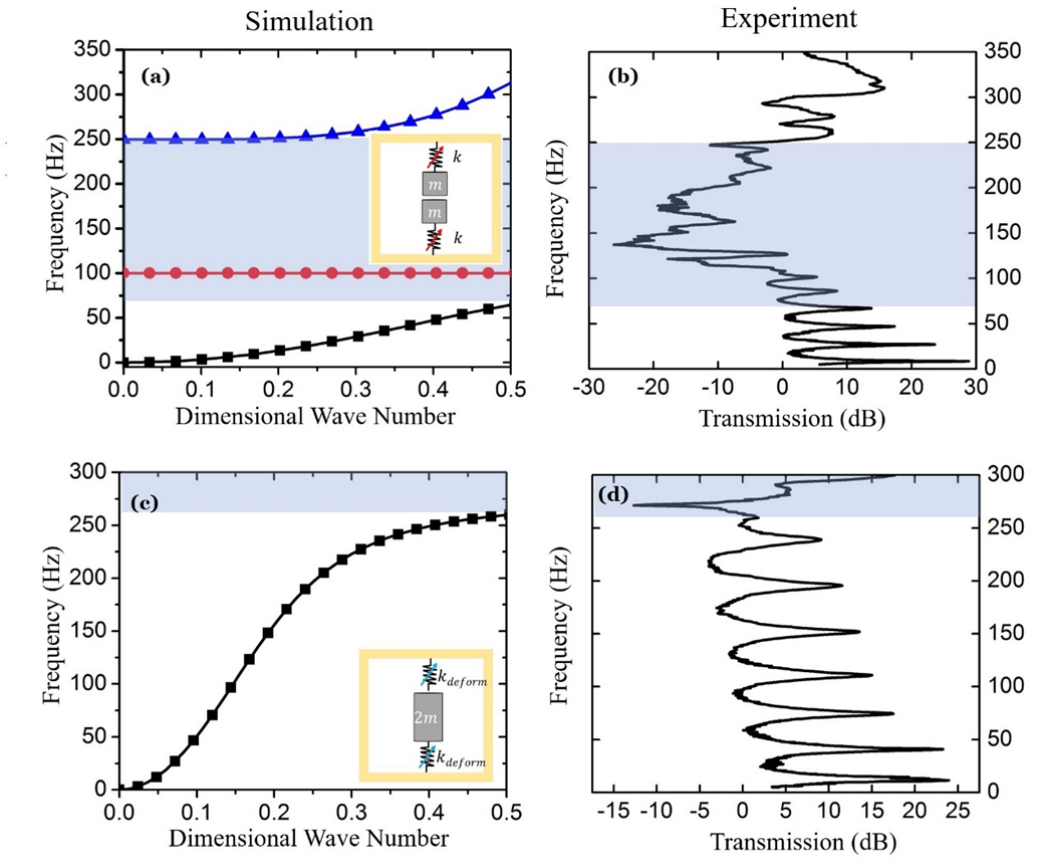

Figure 3 Simulated dispersion and measured frequency-dependent transmission for the samples. Both numerical Fig. 3 (a) and (c) and experimental Fig. 3 (b) and (d) results are shown. The gray regions in in each subplot highlight the band gap.

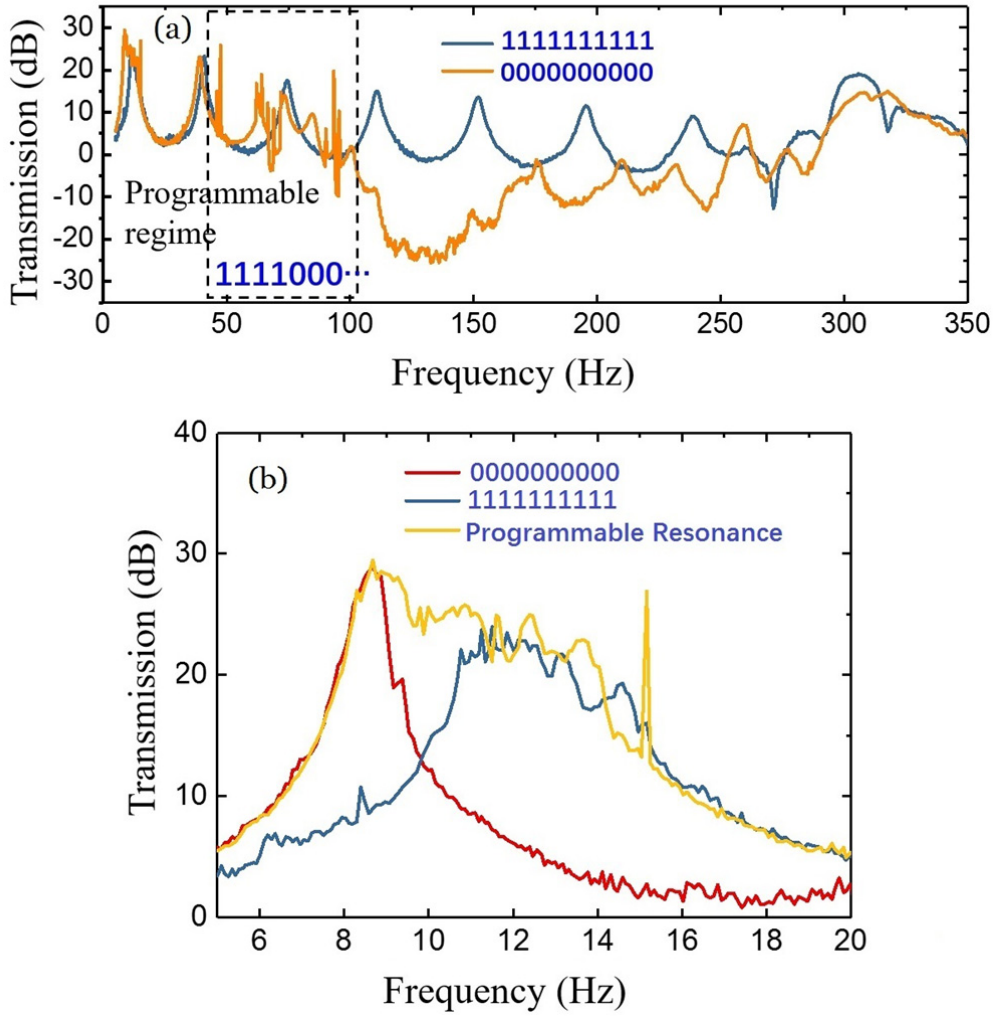

Figure 4. Real-time programmable dynamics during operation: (a) Programmable band gap. The dark-blue line denotes the transmission of the metamaterial with ten switched on unit cells. The orange line denotes the transmission with a dynamic switching process. The switching regime is shown in the dashed rectangle. (b) Programmable resonance. The dark blue and red lines indicate the first resonance when switched on and off, respectively. The yellow line denotes the dynamic switching during operation between the two states.